

In-plane electric polarization of bilayer graphene nanoribbons by interlayer bias voltage

Ryo Okugawa,¹ Junya Tanaka,¹ Takashi Koretsune,² Susumu Saito,^{1,3} and Shuichi Murakami^{1,3}

¹*Department of Physics, Tokyo Institute of Technology,
2-12-1 Ookayama, Meguro-ku, Tokyo 152-8551, Japan*

²*RIKEN Center for Emergent Matter Science, Hirosawa 2-1, Wako, Saitama 351-0198, Japan*

³*TIES, Tokyo Institute of Technology, 2-12-1 Ookayama, Meguro-ku, Tokyo 152-8551, Japan*

We theoretically show that an interlayer bias voltage in the AB-stacked bilayer graphene nanoribbons with armchair edges induces an electric polarization along the ribbon. Both tight-binding and *ab initio* calculations consistently indicate that when the bias voltage is weak, the polarization shows opposite signs depending on the ribbon width modulo three. This nontrivial dependence is explained using a two-band effective model. A strong limit of the bias voltage in the tight-binding model shows either one-third or zero polarization, which agrees with topological argument.

PACS numbers: 72.80.Vp, 73.63.-b, 77.22.Ej, 73.23.-b

Monolayer graphene nanoribbons (GNRs) show various energy bands depending on the edge orientation and the width of the nanoribbons [1, 2]. When the GNRs have armchair edges, the energy bands become gapped or gapless, depending on the width. Like monolayer GNRs, the energy bands in the AB-stacked bilayer GNRs (Fig. 1) also depend sensitively on the edges. Namely, the zigzag bilayer GNRs show localized edge states [3], whereas the armchair bilayer GNRs vary from insulator ($N = 3l$ or $3l + 1$, l : integer) to metal ($N = 3l + 2$) by changing the width N in a tight-binding (TB) model (Fig. 1) [1]. In addition, external fields play scientifically and technologically important roles in atomic-layer materials, such as bilayer graphene. The external electric field opens up the fundamental gap in the AB-stacked bilayer graphene [5, 6] which otherwise possesses massive and gapless parabolic bands in the low energy region [5].

In this Letter, we theoretically show that an external interlayer bias voltage in the AB-stacked bilayer GNR with armchair edges induces a polarization along the ribbon direction. We use two methods: calculation on the TB model and *ab initio* calculations. Both two methods consistently show that when the bias voltage is weak, the polarization shows a nontrivial dependence on the ribbon width, having opposite signs depending on the width modulo three. A strong limit of the bias voltage shows either one-third or zero polarization in the unit of the electron charge, which agrees with topological argument. We then discuss that the present theory applies to a wide variety of atomic-layer compounds. Thus nanostructure which breaks bulk symmetries allows novel responses which are absent in the bulk.

We first discuss symmetry requirement for the transverse response of the polarization along the ribbon induced by the interlayer bias. We take the x and z axis in the direction normal to the edges and the bilayer, respectively, and the y axis along the ribbon (Fig. 1). For armchair or chiral edges, when the interlayer bias voltage is zero, inversion and C_{2x} symmetries are preserved,

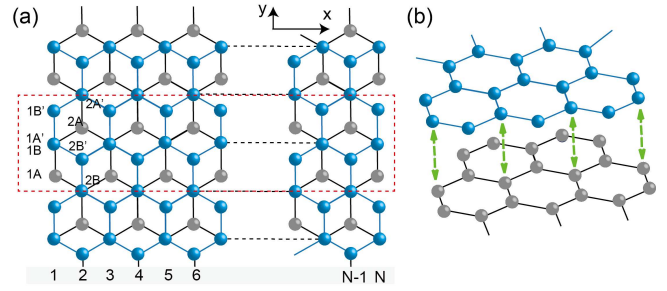


FIG. 1. (Color online) Structure of the AB-stacked bilayer GNR with the armchair edges. (a),(b) The black (blue) lines represents the bondings in the lower (upper) layer. (a) N is the width corresponding to a number of rows. The unit cell of the ribbons (red dashed-line box) contains $4N$ atoms. $nA(A')$ and $nB(B')$ represent the sublattice in the lower (upper) layer within n th row. (b) The green arrows denote the interlayer hoppings between the nB and nA' sites forming “dimers”.

which prohibit emergence of polarization. Interlayer voltage breaks both symmetries, resulting in a polarization along the ribbon. For zigzag edges, xz -plane mirror symmetry is preserved in addition to inversion symmetry, and it prohibits emergence of polarization along the ribbon (y) direction. Because the interlayer voltage does not break this mirror symmetry, it does not induce polarization for zigzag ribbons.

First we numerically calculate the polarization for a spinless TB model.

$$H = \sum_{(i,j)} t_{ij} c_i^\dagger c_j + \frac{U}{2} \sum_i \xi_i c_i^\dagger c_i. \quad (1)$$

The first term describes the hoppings with the amplitude t_{ij} , for which we only consider the nearest-neighbor intralayer hopping t and the interlayer hopping t_\perp within a “dimer”. Here, we set $t_\perp = 0.13t$ ($t > 0$) according to Ref 7. The second term represents the interlayer bias U and ξ_i takes $+1$ (-1) for the upper (lower) layers.

From the TB model, we calculate the electronic contribution of the polarization P in terms of the Berry connection within the modern theory of polarization [2–4]. It is calculated as a change of polarization $P(U) - P(0)$ by changing the interlayer bias voltage U . This calculation works only for insulators, and therefore we restrict ourselves to the insulating GNRs whose width is $N = 3l$ or $3l + 1$ (l : integer). Because $P(0) = 0$ by inversion symmetry, we obtain $P(U)$ numerically.

Using this method, we find that in the bilayer GNRs with the armchair edges, the polarization arises for nonzero interlayer bias voltage U . Figures 2(a)(b) are our numerical results for various widths N . In reality, feasible values of U may be limited to about $|U| < 0.15t$; nevertheless we show the results for much larger U in the figure, to show consistency for the large U limit. Interestingly, the behavior of the polarization is classified into two classes, $N = 3l$ and $N = 3l + 1$. For $N = 3l$, the polarization goes to zero for $U \rightarrow \pm\infty$, while for $N = 3l + 1$ the polarization goes to $\pm e/3$, where $-e$ ($e > 0$) represents the electron charge. Furthermore, the slope around $U \sim 0$ has opposite signs between the two classes. The slope at $U \sim 0$ is steeper for wider ribbons. In the intermediate range of U the polarization oscillates as U is changed. This oscillation accompanies a change of band structure around the Fermi energy, formed by a number of minibands from a finite-size effect.

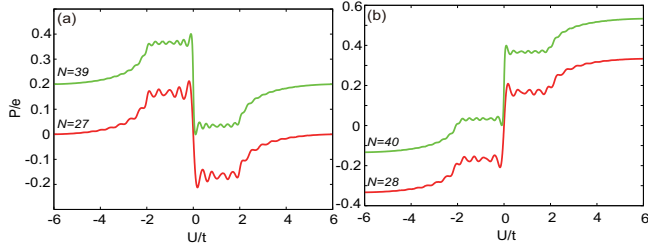


FIG. 2. (Color online) Numerical results of the polarization from the TB model in response to the interlayer bias. The interlayer hopping parameter $t_{\perp} = 0.13t$ is fixed. (a) $N = 3l$ ($N = 27, 39$) and (b) $N = 3l + 1$ ($N = 28, 40$). The results for $N = 39, 40$ (green) are vertically offset by 0.2.

The dependence of the asymptotic behavior at $U \rightarrow \pm\infty$ on the ribbon width can be physically understood as follows. Because there are two electrons per row in the unit cell, two electrons lie on the lower layer under the strong interlayer bias voltage $U \sim +\infty$. As a result, compared from $U \sim 0$, the two electrons are displaced by $a/6$ on average, and therefore the polarization is $P \equiv (a/6) \cdot 2Ne/a = Ne/3 \pmod{e}$ per unit length (Fig. 3), where a is the lattice constant. Here the polarization is defined modulo e [2–4]. Hence we obtain $P \equiv 0 \pmod{e}$ and $P \equiv e/3 \pmod{e}$ for $N = 3l$ and $3l + 1$, respectively. It totally agrees with our numerical calculations.

Next, we focus on the region of the weak interlayer bias voltage in Fig. 2. To understand the novel behavior of

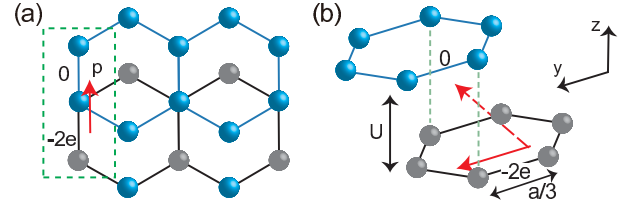


FIG. 3. (Color online) Emergence of the electric dipole moment in the strong limit of the interlayer bias voltage U . (a) and (b) show top and side views of a part of the nanoribbon. 0 and $-2e$ represent the charge at each layer for large U . The dashed and solid red arrows represent the whole and the y component of the dipole moment.

the slope, we construct a simple two-band (2B) effective Hamiltonian for the weakly biased GNRs, by retaining only the highest occupied band and the lowest unoccupied band. To this end, we begin with the analytic forms of the eigenstates of the TB model at $k = 0$ and $U = 0$ [1]. The eigenvalue equation at $k = 0$, $U = 0$ is written

$$\begin{pmatrix} 0 & t(2 \cos \theta + 1) \\ t(2 \cos \theta + 1) & \pm t_{\perp} \end{pmatrix} \begin{pmatrix} A^{\pm} \\ B^{\pm} \end{pmatrix} = \varepsilon^{\pm} \begin{pmatrix} A^{\pm} \\ B^{\pm} \end{pmatrix} \quad (2)$$

where A^{\pm} corresponds to the sum and the difference between the amplitudes at the A and B' sublattices, respectively, and B^{\pm} is defined similarly for the B and A' sublattices (see the Supplemental Material [11] for details). θ is a phase difference of an electronic wave between the neighboring rows, forming a standing wave in the ribbon. Its eigenvalues are

$$\varepsilon^{\pm, q} = \pm \frac{t_{\perp}}{2} + q \sqrt{\left(\frac{t_{\perp}}{2}\right)^2 + t^2(2 \cos \theta + 1)^2}, \quad (3)$$

where $q = \pm 1$. From the boundary condition, we get $\theta = \theta_r^N = \frac{r}{N+1}\pi$, $r = 1, 2, \dots, N$. Here, response of the polarization P to an external perturbation is given by the Berry curvature[3, 4, 12]. Therefore, the eigenstates close to $k = 0$, where the band structure has a direct gap when $U \sim 0$, contributes considerably to the polarization. Hence, from the analytic forms of the eigenstates of the TB model at $k = 0$ and $U = 0$ [1], we retain only the lowest unoccupied state $|+\rangle$ and the highest occupied state $|-\rangle$. Their energy eigenvalues are given by $\pm g_0$, where $g_0 = -t_{\perp}/2 + d$, $d = \sqrt{(t_{\perp}/2)^2 + t^2(2 \cos \theta_{2l+1}^N + 1)^2}$, and $\theta_{2l+1}^N = \pi(2l+1)/(N+1)$ for both $N = 3l$ and $N = 3l + 1$. By using these two eigenstates, we construct a 2B model which describes the energy bands around the Fermi energy when $k \sim 0$ and $U \ll t, t_{\perp}$. The 2B Hamiltonian to the first order in k and U is derived as

$$H_{\text{eff}} = h_1 U \sigma_x + h_2 k \sigma_y + g_0 \sigma_z, \quad (4)$$

where $h_1 = t_{\perp}/(4d)$, $h_2 = at^2(\cos \theta_{2l+1}^N - 1)(2 \cos \theta_{2l+1}^N + 1)/(3d)$ and $\sigma_{x,y,z}$ are the Pauli matrices for the space spanned by the eigenstates $|\pm\rangle$ [11]. We note that width

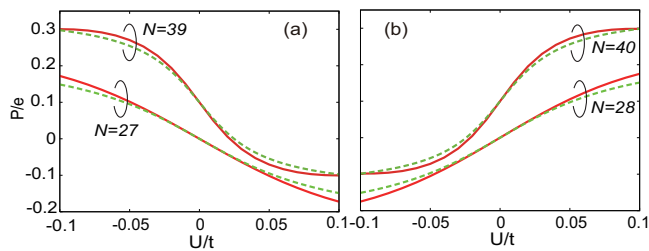


FIG. 4. (Color online) Comparison between the results from the TB model (red solid line) and the 2B model (green dashed line). (a) $N = 3l$ ($N = 27, 39$) and (b) $N = 3l + 1$ ($N = 28, 40$). The results for $N = 39, 40$ are vertically offset by 0.1.

dependence appears through θ_{2l+1}^N . From the 2B Hamiltonian, we calculate the polarization $P(U)$ for small U , as shown in Fig 4. They well agree with the results of the TB model in the $U \sim 0$ region, including the sign of the slope, for $N > 20$. For $N < 20$, the gap in the TB model is non-monotonous as a function of the interlayer bias U ; for small U the gap decreases as a function of U . It is not reproduced in the 2B model where the gap always increases with U . This leads to differences between the two models.

The width dependence is understood from the analytic formula for the slope of $P(U)$:

$$\frac{\partial P}{\partial U} = \frac{ie}{2\pi} \int_{-\pi/a}^{\pi/a} dk \frac{\langle u_{k-} | \frac{\partial H}{\partial k} | u_{k+} \rangle \langle u_{k+} | \frac{\partial H}{\partial U} | u_{k-} \rangle}{(E_{k-} - E_{k+})^2} + c.d. \quad (5)$$

Here E_{k_j} and $|u_{k_j}\rangle$ are the eigenvalue and the eigenstate of the 2B Hamiltonian for the j band. Therefore, the slope at $U = 0$ is

$$\left. \frac{\partial P}{\partial U} \right|_{U=0} = -\frac{e}{2a} h_1 h_2 \frac{1}{g_0 \sqrt{g_0^2 + (h_2 \pi/a)^2}}, \quad (6)$$

and its sign is given by $-\text{sgn}(h_2)$. From $2\pi/3 - \theta_{2l+1}^N = \mp\pi/(3N+3)$ for $N = 3l$ and $3l+1$, the sign of the slope is negative for $N = 3l$ and positive for $N = 3l+1$, in agreement with the results for various widths of GNRs. Asymptotic form for a wider ribbon is evaluated as

$$\left. \frac{\partial P}{\partial U} \right|_{U=0} \sim \pm \frac{3t_{\perp} e}{8\pi^3 t^2} (N+1)^2. \quad (7)$$

where the signs \pm is $-$ for $N = 3l$ and $+$ for $N = 3l+1$.

These behaviors are confirmed by *ab initio* calculations based on density functional theory (DFT). We perform the electronic structure calculation of hydrogen terminated AB-stacked bilayer GNRs within the local-density approximation (LDA)[13, 14] based on DFT using QUANTUM ESPRESSO package [15]. We use ultra-soft pseudopotentials[16] and plane-wave basis sets to describe the charge densities and wave functions with cutoff energies of 30Ry and 300Ry, respectively. The supercell approach is used and the distances of neighboring bilayer

GNRs along the x -axis and the z -axis are at least 10 and 30 Å, respectively. The geometries are fully optimized. To discuss the effect of the external electric field, we apply a periodic zigzag potential along the z -axis in the supercell. Under the external field, E , we obtain the band structure with $48 \times 1 \times 1$ k-points and calculate the electric polarization in terms of the Berry connection.

The dot symbols in Fig. 5 (a),(b) represent the DFT results on polarization for hydrogen terminated AB-stacked bilayer GNRs under the electric field E . Here, we put $P(E=0) = 0$ by symmetry. Apparently, the signs of the slopes of P obtained by DFT calculations completely agree with those from the TB and the 2B model. Furthermore, the N dependence of the polarization, *i.e.*, $\partial P(U)/\partial U|_{U=0} \propto (N+1)^2$ in Eq. (7), is well reproduced in the DFT results (see Fig. 5 (c)). These indicate that the simple TB model, and consequently its 2B effective model, well capture the key features of the polarization in this system. To compare the polarization values with the TB model quantitatively, we relate the electric field, E to the on-site energies U in the TB model. To this end, we construct maximally localized Wannier functions for the valence bands using carbon σ and π orbitals[17–19], and the result is shown in Fig. 5 (d). The obtained on-site energies for π orbitals in each layer are almost independent of the position of the orbitals except at the edges. Thus, in Fig. 5 (d), we use average values excluding the edges.

As shown in Fig. 5 (d), we find that for weak electric field $|E| < 0.2\text{V}/\text{\AA}$, E and U are almost linear, whereas their proportionality constant depends on the ribbon width. Using this correspondence the results on the TB model over various U is translated into the dependence on the electric field E , as shown as the dotted lines in Fig. 5 (a) and (b). We notice that the result from DFT and that from the TB models have similar tendencies, whereas they are different by a factor of two smaller or larger, depending on the series $N = 3l$ and $N = 3l+1$. This difference between DFT and the TB model can be partly attributed to the difference of the gap size. In the result of the 2B model in Eq. (6), the polarization is inversely proportional to the gap size, because $h_2 \pi/a$ is much larger than g_0 for the given parameters. Actually, the gap size obtained from DFT is smaller (larger) than that of the TB model for $N = 3l$ ($N = 3l+1$) even at $U = 0$. Therefore, in order to incorporate this difference of the gap size, we rescale the results of the polarization of the TB model by the ratio between the gaps from the DFT and that of the TB model. This rescaling enhances (suppresses) the polarization for $N = 3l$ ($N = 3l+1$). After the rescaling, the results (solid lines in Fig. 5 (a) and (b)) exhibits better agreement with the DFT results. Thus despite the simplicity of the TB model, it describes the various aspects of the behavior of the polarization well including the width dependence.

To experimentally measure this proposed effect, one

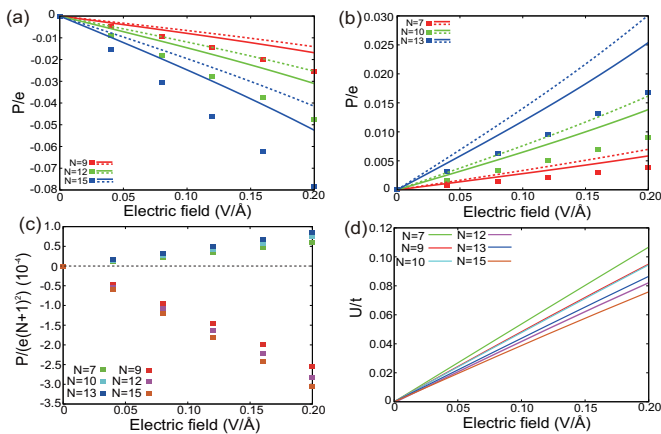


FIG. 5. (Color) Comparison between the results of DFT calculations and those with the TB model. (a), (b) Polarization obtained by DFT calculations (squares) compared with results with the TB model (lines). The results of the TB with (without) rescaling by the gap size are shown as a solid line (dotted line) (see text). (a) ($N = 9, 12, 15$) are for $N = 3l$, and (b) ($N = 7, 10, 13$) are for $N = 3l + 1$. Note that it is for a spinless system, and the results here should be multiplied by two to compare with experiments. (c) Induced polarization P by DFT calculation divided by $(N + 1)^2$. (d) Relationship between out-of-plane electric field $|\mathbf{E}|$ versus on-site potential energy difference U . U is scaled by the hopping amplitude $t = 2.6\text{eV}$ [7].

needs a bilayer nanoribbon with well-defined edges and width. For single-layer graphene nanoribbons, well-defined edge orientations have been demonstrated [20–23], and it might be realized also for bilayer graphene. For the bilayer graphene, interlayer electric field up to $0.3\text{V}/\text{\AA}$ has been achieved [24], and therefore the proposed effect with polarization up to $\sim -0.12e$ per spin for $N = 15$ is expected to be realizable experimentally. We also have calculated the effect of periodic modulations of the width to check the edge disorder effect via supercell approach and confirmed that the polarization survives the weak modulations considered [11]. Nevertheless, since the effect is sensitive to the ribbon width, the proposed effect will disappear in the presence of strong disorder. We note here that the in-plane polarization by an interlayer bias can be expected for a wide variety of atomic-layer compounds, as long as the symmetry criterion for its emergence is satisfied. As an example, a bilayer armchair ribbon of transition metal dichalcogenides in the 2H stacking satisfies this criteria. Moreover, our calculation show induced polarization in AA'-stacked bilayer boron nitride nanoribbons [11]. Such a wide choice of candidate materials provides us with many chances for experimental verifications of our theory.

To conclude, we theoretically show that the AB-

stacked graphene nanoribbon with armchair edges has a polarization along the ribbon direction, when interlayer bias voltage is applied. This is shown both by the simple tight-binding model and the *ab initio* calculations. In particular, the linear response to the interlayer voltage shows different signs for the cases $N = 3l$ and $N = 3l + 1$, and it is fully understood by means of a simple two-band model.

This work is partially supported by Grant-in-Aid from MEXT, Japan (No. 26287062, No. 25107005 and No. 25104711), JSPS Research Fellowships for Young Scientists, and MEXT Elements Strategy Initiative to Form Core Research Center (TIES).

-
- [1] M. Fujita, K. Wakabayashi, K. Nakada, K. Kusakabe, J. Phys. Soc. Jpn. **65**, 1920 (1996).
 - [2] K. Wakabayashi, M. Fujita, H. Ajiki, M. Sigrist, Phys. Rev. B **59**, 8271 (1999).
 - [3] E. V. Castro, N. M. R. Peres, J. M. B. Lopes dos Santos, A. H. Castro Neto, F. Guinea, Phys. Rev. Lett. **100**, 026802 (2008).
 - [4] B. Sahu, H. Min, A. H. MacDonald, S. K. Banerjee, Phys. Rev. B **78**, 045404 (2008).
 - [5] E. McCann, V. I. Fal'ko, Phys. Rev. Lett. **96**, 086805 (2006).
 - [6] E. McCann, Phys. Rev. B **74**, 161403 (2006).
 - [7] H. Min, B. Sahu, S. K. Banerjee, A. H. MacDonald, Phys. Rev. B **75**, 155115 (2007).
 - [8] R. D. King-Smith, D. Vanderbilt, Phys. Rev. B **47**, 1651 (1993).
 - [9] R. Resta, Ferroelectrics **136**, 51 (1992).
 - [10] R. Resta, Rev. Mod. Phys. **66**, 899 (1994).
 - [11] See the Supplemental Material.
 - [12] M. V. Berry, Proc. Roy. Soc. London Ser A **392**, 45 (1984).
 - [13] D. M. Ceperley, B. J. Alder, Phys. Rev. Lett. **45**, 566 (1980).
 - [14] J. P. Perdew, A. Zunger, Phys. Rev. B **23**, 5048 (1981).
 - [15] P. Giannozzi *et al.*, J. Phys.: Condens. Matter **21**, 395502 (2009).
 - [16] D. Vanderbilt, Phys. Rev. B **41**, 7892 (1990).
 - [17] N. Marzari, D. Vanderbilt, Phys. Rev. B **56**, 12847 (1997).
 - [18] I. Souza, N. Marzari, D. Vanderbilt, Phys. Rev. B **65**, 035109 (2001).
 - [19] A. A. Mostofi *et al.*, Comput. Phys. Commun. **178**, 685 (2008).
 - [20] G. Z. Magda *et al.*, Nature **514**, 608 (2014).
 - [21] M. Y. Han, B. Özyilmaz, Y. Zhang, P. Kim, Phys. Rev. Lett. **98**, 206805 (2007).
 - [22] J. Cai *et al.*, Nature **466**, 470 (2010).
 - [23] D. Kosynkin *et al.*, Nature **458**, 872 (2009).
 - [24] Y. Zhang *et al.*, Nature **459**, 820 (2009).

FORMULA OF THE POLARIZATION IN TERMS OF THE BLOCH WAVEFUNCTIONS

In our calculation of the polarization P in terms of the Bloch wavefunctions, we used the formula [2–4]

$$P = -\frac{ie}{2\pi} \int_{-\frac{\pi}{a}}^{\frac{\pi}{a}} dk \sum_n^{\text{occ.}} \langle u_{kn} | \frac{\partial}{\partial k} | u_{kn} \rangle, \quad (\text{S1})$$

where $|u_{kn}\rangle$ is the Bloch wavefunction satisfying the cell-periodic gauge condition

$$u_{k,n}(\mathbf{r}) = e^{iGy} u_{k+G,n}(\mathbf{r}), \quad (\text{S2})$$

and the summation is taken over the occupied states below the Fermi energy. Here k is the Bloch wavenumber and $G \equiv 2\pi/a$ is a reciprocal lattice vector. In numerical calculation, the differentiation in terms of k in Eq. (S1) should be replaced by a difference in k . Such a formula with this replacement is discussed in detail in Ref. 3, and we followed this formalism for the calculation of the polarization.

POLARIZATION CALCULATED FROM THE TIGHT-BINDING MODEL FOR VARIOUS WIDTHS

We show numerical results of the polarization induced by the interlayer bias for graphene nanoribbons (GNRs) with various widths N , calculated from the tight-binding model. Some results are shown in Fig. 2 in the main text, and we show more examples for various N in Fig. S1. For $N = 3l$ the results are shown in Fig. S1a, c ($N = 9, 15, 21$), and in Fig. 2a, b ($N = 27, 39$). For $N = 3l + 1$ the results are shown in Fig. S1b, d ($N = 10, 16, 22$), and in Fig. 2c, d ($N = 28, 40$). In the wide range of U (Fig. S1), the polarization P oscillates as a function of U , which is attributed to crossings of minibands. There are more oscillations for larger N , which reflects the fact that there are a larger number of minibands for wider ribbons. On the other hand, the oscillation amplitude becomes gradually smaller for wider ribbons (see Fig. 2) because the contribution from each miniband becomes relatively smaller. On the other hand, in the regime $U \sim 0$, we showed from the two-band model that the polarization is linear in U with its slope scales with $(N + 1)^2$. This is roughly reproduced for the results shown in Fig. S1c and d.

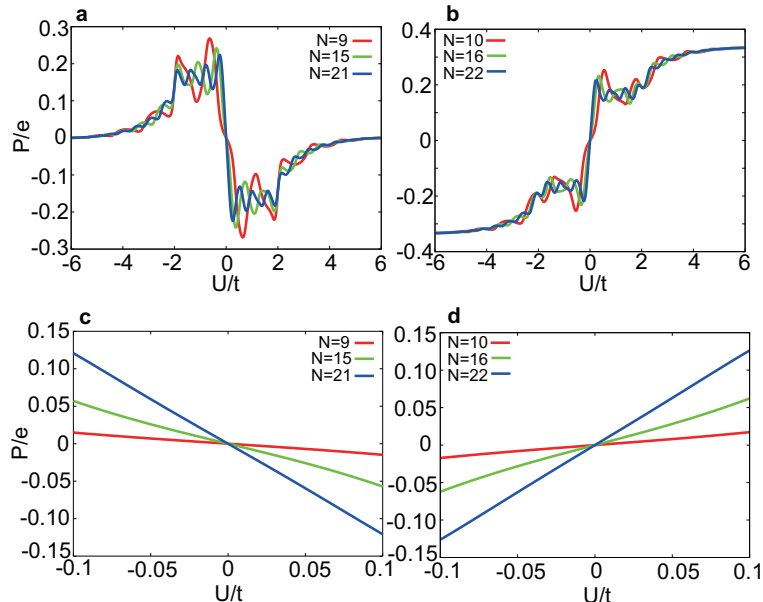


FIG. S1. Polarization induced by the interlayer bias U for GNRs with various widths N , calculated from the tight-binding model. It is shown as a function of the interlayer bias U . a and c are for the class $N = 3l$ and b and d are for the class $N = 3l + 1$.

It may look strange that for a large N limit, i.e. the 2D graphene limit, the polarization has a different asymptotics for $N = 3l$ and $N = 3l + 1$. It is in fact reasonable; the polarization per area is proportional to P divided by the width, and therefore goes to zero for $N \rightarrow \infty$.

EIGENVALUES AND EIGENVECTORS OF THE TIGHT-BINDING MODEL

Here we derive the two-band low-energy effective Hamiltonian from the eigenstates of the tight-binding model of the bilayer GNR with armchair edge, without the interlayer bias voltage:

$$H_t = \sum_{\langle i,j \rangle} t_{ij} c_i^\dagger c_j. \quad (\text{S3})$$

Firstly, to obtain the two-band Hamiltonian, we diagonalize the tight-binding model at $k = 0$ according to Ref. 1. We set the eigenvector of the Hamiltonian

$$|\Phi(k=0)\rangle = \sum_{m=1}^N a_m |mA\rangle + \sum_{m=1}^N b_m |mB\rangle + \sum_{m=1}^N a'_m |mA'\rangle + \sum_{m=1}^N b'_m |mB'\rangle, \quad (\text{S4})$$

where A and B represent sublattices in the lower layer, and A' and B' in the upper layer. Here, a_m , b_m , a'_m , and b'_m are expansion coefficients. From the tight-binding model at $k = 0$, we obtain

$$\varepsilon a_m = t(b_{m-1} + b_m + b_{m+1}), \quad (\text{S5})$$

$$\varepsilon b_m = t(a_{m-1} + a_m + a_{m+1}) + t_\perp a'_m, \quad (\text{S6})$$

$$\varepsilon a'_m = t(b'_{m-1} + b'_m + b'_{m+1}) + t_\perp b_m, \quad (\text{S7})$$

$$\varepsilon b'_m = t(a'_{m-1} + a'_m + a'_{m+1}), \quad (\text{S8})$$

where ε represents the energy eigenvalue. To solve the above equations (S5)-(S8), we introduce new coefficients

$$\alpha_m^\pm = \frac{1}{\sqrt{2}}(a_m \pm b'_m), \quad \beta_m^\pm = \frac{1}{\sqrt{2}}(b_m \pm a'_m). \quad (\text{S9})$$

Then, we obtain

$$\varepsilon \alpha_m^\pm = t(\beta_{m-1}^\pm + \beta_m^\pm + \beta_{m+1}^\pm), \quad (\text{S10})$$

$$\varepsilon \beta_m^\pm = t(\alpha_{m-1}^\pm + \alpha_m^\pm + \alpha_{m+1}^\pm) \pm t_\perp \beta_m^\pm. \quad (\text{S11})$$

Since $\alpha_0^\pm = 0 = \beta_0^\pm$, the solutions have the form $\alpha_m^\pm \propto A^\pm \sin(m\theta)$ and $\beta_m^\pm \propto B^\pm \sin(m\theta)$, where θ is a constant ($0 < \theta < \pi$). We rewrite the equations (S10) and (S11) in the matrix form

$$\begin{pmatrix} 0 & t(2 \cos \theta + 1) \\ t(2 \cos \theta + 1) & \pm t_\perp \end{pmatrix} \begin{pmatrix} A^\pm \\ B^\pm \end{pmatrix} = \varepsilon^\pm \begin{pmatrix} A^\pm \\ B^\pm \end{pmatrix}, \quad (\text{S12})$$

and its eigenvalues are obtained analytically.

$$\varepsilon^{\pm,q} = \pm \frac{t_\perp}{2} + q \sqrt{\left(\frac{t_\perp}{2}\right)^2 + t^2(\cos \theta + 1)^2}, \quad (\text{S13})$$

where $q = \pm 1$. From the boundary condition, the coefficients must vanish when $m = 0$ and $N + 1$ and we get

$$\theta_r = \frac{r}{N+1} \pi, \quad r = 1, 2, \dots, N. \quad (\text{S14})$$

Thus, we get $4N$ eigenvalues and eigenvectors,

$$\varepsilon_r^{\pm,q} = \pm \frac{t_\perp}{2} + q d_r, \quad (\text{S15})$$

$$\begin{pmatrix} A_r^{\pm,q} \\ B_r^{\pm,q} \end{pmatrix} = \frac{1}{\sqrt{2d_r(d_r \mp q \frac{t_\perp}{2})}} \begin{pmatrix} \mp \frac{t_\perp}{2} + q d_r \\ t(2 \cos \theta_r + 1) \end{pmatrix}. \quad (\text{S16})$$

We put $d_r = \sqrt{(t_\perp/2)^2 + t^2(2 \cos \theta_r + 1)^2}$ for notational simplicity. These energy eigenvalues can become zero only when $\cos \theta_r = -1/2$. When $N = 3l + 2$ it can be satisfied for $r = 2l + 2$, and the energy bands are gapless at $k = 0$ because $\varepsilon_{2l+2}^{-,+} = \varepsilon_{2l+2}^{+,-} = 0$. On the other hand, when $N = 3l$ or $3l + 1$, $\cos \theta_r = -1/2$ cannot be satisfied the energy bands are gapped. Therefore, the polarization $P_y(U)$ can be defined in the nanoribbons with widths $N = 3l$ or $3l + 1$. In these cases, the energy eigenvalues closest to zero are $\varepsilon_{2l+1}^{-,+}$ and $\varepsilon_{2l+1}^{+,-}$, and the corresponding eigenstates

$|+\rangle \equiv |r = 2l + 1, -, +\rangle$ and $|-\rangle \equiv |r = 2l + 1, +, -\rangle$ considerably contribute to the polarization. For brevity, we write $\pm g_0 = \varepsilon_{2l+1}^{\mp, \pm}$, and

$$g_0 = -\frac{t_{\perp}}{2} + d_{2l+1}, \quad (\text{S17})$$

$$|\pm\rangle = \frac{1}{\sqrt{2 \sum_{m=1}^N \sin^2(m\theta_{2l+1})}} \times \sum_{m=1}^N \sin(m\theta_{2l+1}) \left(A_{2l+1}^{\mp, \pm} (|mA\rangle \mp |mB'\rangle) + B_{2l+1}^{\mp, \pm} (|mB\rangle \mp |mA'\rangle) \right). \quad (\text{S18})$$

Hereafter, we omit subscripts $2l + 1$ except for that in θ_{2l+1} ; for example, we write $d = d_{2l+1}$.

CONSTRUCTION OF THE TWO-BAND HAMILTONIAN

To elucidate the polarization in the weak interlayer bias voltage, we construct a two-band low-energy effective Hamiltonian for the space spanned by $|\pm\rangle$. Therefore, we add the interlayer bias voltage U to the tight-binding model as a perturbation;

$$H_U = \frac{U}{2} \sum_i \xi_i c_i^{\dagger} c_i, \quad (\text{S19})$$

We retain terms up to the linear order in k and the nonzero matrix elements to this order are given by

$$\begin{aligned} \langle mA | H_t | nB \rangle &= \langle mA' | H_t | nB' \rangle \\ &= t(\delta_{m,n-1} + \delta_{m,n} + \delta_{m,n+1}) + ikt \frac{a}{3} (\delta_{m,n} - \frac{1}{2}\delta_{m-1,n} - \frac{1}{2}\delta_{m+1,n}), \end{aligned} \quad (\text{S20})$$

$$\langle mA' | H_t | nB \rangle = t_{\perp} \delta_{m,n}, \quad (\text{S21})$$

$$\langle mA | H_U | nA \rangle = \langle mB | H_U | nB \rangle = -\frac{U}{2} \delta_{m,n}, \quad (\text{S22})$$

$$\langle mA' | H_U | nA' \rangle = \langle mB' | H_U | nB' \rangle = \frac{U}{2} \delta_{m,n}. \quad (\text{S23})$$

Therefore, the nonzero matrix elements of H_t and H_U are

$$\langle \pm | H_t | \pm \rangle = \pm g_0, \quad (\text{S24})$$

$$\langle + | H_t | - \rangle = ikt^2 \frac{a}{3d} (1 - \cos \theta_{2l+1}) (2 \cos \theta_{2l+1} + 1), \quad (\text{S25})$$

$$\langle + | H_U | - \rangle = \frac{Ut_{\perp}}{4d}. \quad (\text{S26})$$

Hence, we obtain the two-band Hamiltonian $H_{\text{eff}} = H_t + H_U$,

$$H_{\text{eff}}(k, U) = h_1 U \sigma_x + h_2 k \sigma_y + g_0 \sigma_z, \quad (\text{S27})$$

where

$$h_1 = \frac{t_{\perp}}{4d}, \quad h_2 = -t^2 \frac{a}{3d} (1 - \cos \theta_{2l+1}) (2 \cos \theta_{2l+1} + 1). \quad (\text{S28})$$

The eigenvalues and eigenstates of this two-band Hamiltonian are

$$E_{k,\pm} = \pm \sqrt{(h_1 U)^2 + (h_2 k)^2 + g_0^2} = \pm g, \quad (\text{S29})$$

$$|u_{k,\pm}\rangle = \frac{1}{\sqrt{2g(g \pm g_0)}} \begin{pmatrix} g_0 \pm g \\ h_1 U + ih_2 k \end{pmatrix}. \quad (\text{S30})$$

POLARIZATION FROM THE TWO-BAND HAMILTONIAN

We focus on the region of the weak interlayer bias voltage to clarify the difference of the slope of the polarization at $U \sim 0$ for two classes $N = 3l$ and $N = 3l + 1$. The polarization P is given by [2–4]

$$P = \int_0^U dU' j(U'), \quad (\text{S31})$$

where

$$j(U) = \frac{ie}{2\pi} \int_{-\frac{\pi}{a}}^{\frac{\pi}{a}} dk \sum_n^{\text{occ.}} \sum_m^{\text{unocc.}} \frac{\langle u_{kn} | \frac{\partial H}{\partial k} | u_{km} \rangle \langle u_{km} | \frac{\partial H}{\partial U} | u_{kn} \rangle}{(E_{kn} - E_{km})^2} + c.c. \quad (\text{S32})$$

Here, $j(U) = \partial P / \partial U$, and n and m are band indices for occupied bands and unoccupied bands, respectively. E_{kj} and $|u_{kj}\rangle$ are the j th eigenvalue and the eigenstate of the Hamiltonian. In the present case $n = -$ and $m = +$, and therefore P and $j(U)$ are calculated by using the two-band Hamiltonian derived in section .

$$P(U) = -\frac{e}{2\pi} \arctan \left(\frac{h_1 h_2 U \pi / a}{g_0 \sqrt{g_0^2 + (h_1 U)^2 + (h_2 \pi / a)^2}} \right), \quad (\text{S33})$$

$$j(U) = -\frac{e}{2a} h_1 h_2 \frac{g_0}{((h_1 U)^2 + g_0^2) \sqrt{(h_1 U)^2 + g_0^2 + (h_2 \pi / a)^2}}. \quad (\text{S34})$$

In particular, the slope of the polarization at $U = 0$, i.e. $j(0)$, is given by

$$j(0) = -\frac{e}{2a} h_1 h_2 \frac{1}{g_0 \sqrt{g_0^2 + (h_2 \pi / a)^2}}. \quad (\text{S35})$$

Because $t_{\perp} > 0$, h_1 and g_0 are positive, and we have

$$\text{sgn}(j(0)) = -\text{sgn}(h_2) = \text{sgn}\left(\frac{2}{3}\pi - \theta_{2l+1}\right). \quad (\text{S36})$$

Here,

$$\frac{2}{3}\pi - \theta_{2l+1} = \begin{cases} -\frac{\pi}{3(N+1)} & N = 3l \\ \frac{\pi}{3(N+1)} & N = 3l + 1 \end{cases}. \quad (\text{S37})$$

Therefore, the sign of $j(0) = \partial P / \partial U|_{U=0}$ is given by

$$\frac{\partial P}{\partial U} \Big|_{U=0} \begin{cases} < 0 & N = 3l \\ > 0 & N = 3l + 1 \end{cases}, \quad (\text{S38})$$

which well agrees with the numerical results of the tight-binding model. Asymptotic behavior of $j(0)$ (Eq. (S35)) is evaluated for large N , where $g_0 \ll h_2 \pi / a$;

$$j(0) = -\text{sgn}(h_2) \frac{h_1 e}{2\pi g_0} \sim \pm \frac{t_{\perp} e}{8\pi d(d - \frac{t_{\perp}}{2})}. \quad (\text{S39})$$

where \pm is $-$ for $N = 3l$ and $+$ for $N = 3l + 1$. By using equation (S37) it is approximated as

$$j(0) \sim \pm \frac{3t_{\perp} e}{8\pi 3t^2} (N + 1)^2. \quad (\text{S40})$$

EFFECT OF PERIODIC MODULATION OF THE RIBBON WIDTH

We numerically calculate the polarization in bilayer GNRs with weak periodic modulations of the ribbon widths by using the tight-binding model when the interlayer bias voltage is weak. We consider two cases of periodic modulations by changing the width of each layer in various ways.

Firstly, we discuss an effect of the difference of the widths of the upper and lower layers. Figure S2 shows the polarization in the armchair bilayer GNRs when the upper and lower layers have the different widths. Then, we calculate the polarization by changing the width for the upper layer N_U while fixing that for the lower layer N_L , except that $N_L = 2$ or $N_U = 2 \pmod{3}$ since the energy bands are gapless at $U = 0$. When $N_L = N_U$, the system is the perfectly stacked bilayer armchair GNRs in Fig. 1. The results in Fig. S2 **b** and **c** correspond to the polarization for $N_L = 12 \equiv 0$ and $N_L = 13 \equiv 1 \pmod{3}$, respectively. Consequently, we can see that all the slopes of polarization in Fig. S2 have the same sign regardless of the width of the upper layer N_U . Furthermore, even if the bilayer is composed of two layers with the width 0 and 1 $\pmod{3}$, we find that the sign of the slope is equal to that of the perfectly stacked bilayer GNRs with the narrower width although the magnitude becomes small. Therefore, when the widths of the upper and lower layers are different, the polarization behaves like the perfectly stacked armchair GNRs with the width $\min(N_U, N_L)$.

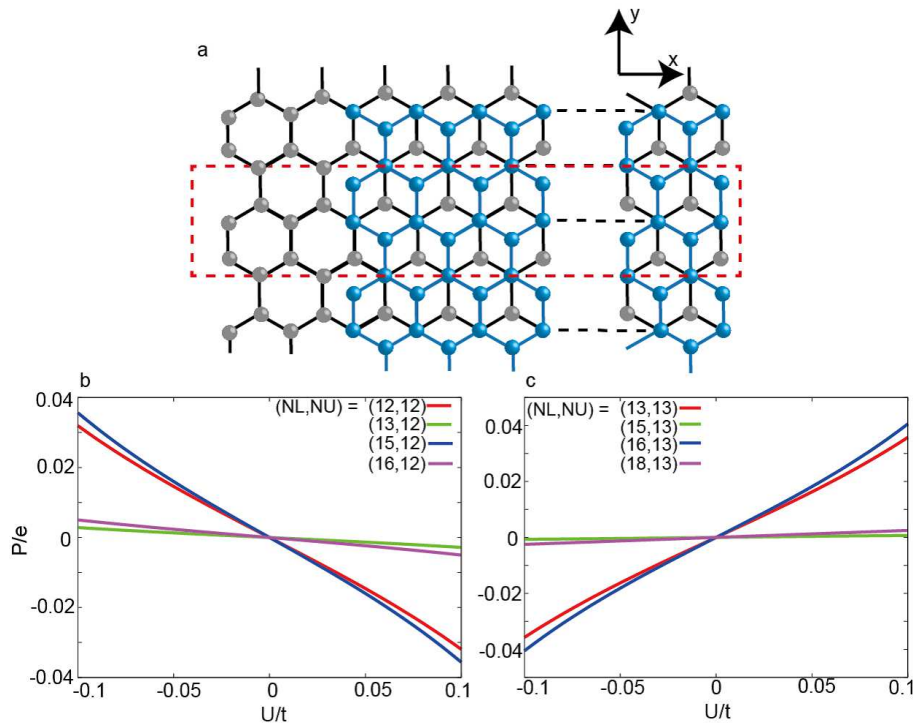


FIG. S2. **Polarization in the bilayer composed of two layers with different widths.** **a** shows structure of the GNRs with the different upper and lower layer. The unit cell is described by the red dashed-line box. **b** and **c** show the polarization for $N_U = 12$ and $N_U = 13$, respectively. **b** is for $N_U = 3l$, and **c** is for $N_U = 3l + 1$.

Secondly, we calculate the polarization of bilayer GNRs when the widths of the upper and lower layers alternates between two values N_1 and N_2 ($N_1 \geq N_2$), as shown in Fig. S3 **a** having no dangling bonds. In this system, the primitive translation vector doubles. In particular, when $N_1 = N_2$, the system corresponds to the armchair bilayer GNRs. In this case, when we calculate the polarization, we change only N_1 and fix N_2 . The results of the polarization for various widths (N_1, N_2) are shown in Fig. S3. Figure S3 **b** and **c** show the polarization for $N_2 = 12 \equiv 0$ and $N_2 = 13 \equiv 1 \pmod{3}$, respectively. As a result, as N_1 becomes larger, we find that the magnitudes of the polarization for $N_2 \equiv 0 \pmod{3}$ are enhanced, while those for $N_2 \equiv 1 \pmod{3}$ are suppressed. Nevertheless, the sign of the slope of the polarization is unchanged from that of the perfect armchair GNRs with the width $N_1 = N_2$. Therefore, we can see that the polarization in the weak interlayer bias voltage is dominated by the narrow part of GNRs, which is similar to the previous case.

From the above results, we find that small variations of the width do not affect the sign of the slope of the polarization in the weak interlayer bias voltage. In other words, even though the edges of the bilayer graphene nanoribbons are not completely perfect, the nontrivial dependence of the polarization on the width appear like the perfectly stacked bilayer GNRs with armchair edges. Thus, the in-plane polarization in response to the interlayer voltage survives even if the edges have weak periodic modulation of the ribbon width, as long as the energy bands are gapped. Nevertheless, since the effect is sensitive to ribbon width, the proposed effect will disappear in the presence of strong disorder.

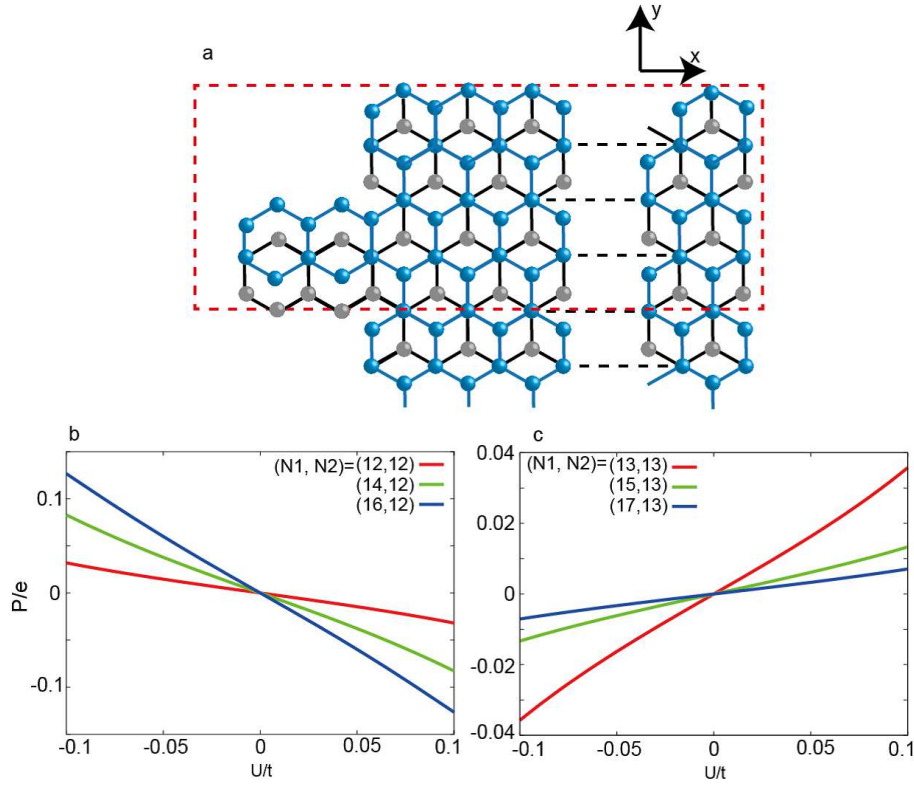


FIG. S3. **Polarization in the bilayer consisting of the stacked monolayer with two widths.** **a** shows the structure of the bilayer nanoribbons with two widths. The red dashed-line box describes the unit cell. **b** and **c** are examples of the polarization for $N_U = 12$ and $N_U = 13$, respectively. **b** is for $N_U = 3l$, and **c** is for $N_U = 3l + 1$.

POLARIZATION IN THE BILAYER BN NANORIBBON

We explained the emergence of the polarization in bilayer graphene nanoribbons by symmetry argument. Therefore, other nanoribbons of atomic-layer compounds can have a finite polarization along the ribbon direction in response to the interlayer voltage, when the symmetry criterion for such a response is satisfied. To confirm this, we compute the polarization of hydrogen terminated bilayer BN nanoribbons from first-principles calculations. Here, we consider so-called AA'-stacked bilayer BN nanoribbons with the armchair edges and the geometry is fully optimized (see Fig. S4 (a)). As in the case of the bilayer armchair GNRs, xz -mirror symmetries are broken in this structure. When the interlayer bias voltage is zero, inversion symmetry is preserved and the polarization is zero. The interlayer voltage breaks the inversion symmetry, leading to nonzero polarization along the ribbon, as we see in the following. Figure S4 (b) shows calculated in-plane polarization as a function of the interlayer voltage. As we can see, a finite polarization appears as expected. Note that the size of the polarization is rather small compared to those in the GNRs. One reason is that the band gaps of these nanoribbons are relatively large (~ 4.3 eV both for $N = 7$ and $N = 9$ at $U = 0$).

-
- [1] Sahu, B., Min, H., MacDonald, A. H. & Banerjee, S. K. Energy gaps, magnetism, and electric-field effects in bilayer graphene nanoribbons. *Phys. Rev. B* **78**, 045404 (2008).
- [2] Resta, R. Theory of the electric polarization in crystals.

Ferroelectrics **136**, 51–55 (1992).

- [3] King-Smith, R. D. & Vanderbilt, D. Theory of polarization of crystalline solids. *Phys. Rev. B* **47**, 1651–1654 (1993).
- [4] Resta, R. Macroscopic polarization in crystalline dielectrics: the geometric phase approach. *Rev. Mod. Phys.* **66**, 899–915 (1994).

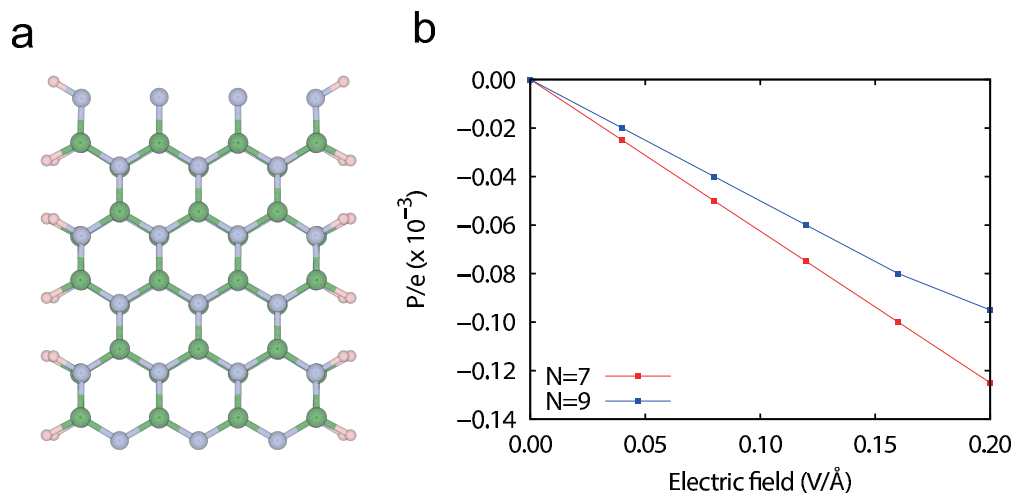


FIG. S4. **Polarization in the BN nanoribbons.** **a** Top view of the hydrogen terminated bilayer BN nanoribbon with the armchair edges for $N = 7$. B (N) atoms on the lower layer are just below the N (B) atoms on the upper layer. **b** Electric field dependence of the polarization obtained by DFT calculations for bilayer BN nanoribbons with the armchair edges.